lattice breakup from grinding, thermal stress, and ambient temperature exposure at the end of the data collection procedure.

The magnetic susceptibility data for form 1 and for the unsolvated β phase are displayed graphically in Figure 7. The plotted data are expressed in terms of the magnetic moment per dimer and the room-temprature moments (2.46 and 2.55 μ_B, respectively) are seen to have values close to the spin-only value of 2.45 μ_B (the square root of the sum of the squares of individual $S = {}^1/_2$ moments of 1.73 μ_B). These values, and those of all the higher temperature points, are, of course, quite sensitive to the value of the diamagnetic correction used: -898 and -806×10^{-6} cgsu/mol of dimer, respectively, for form 1 and the β phase. These values are based on Pascal's constants[29] and do not include the constitutive correction for TPP suggested by Eaton and Eaton[30] because doing so leads to unrealistically high moments ($\sim$2.8 μ_B). It is unknown what the constitutive correction for the TPP$^{\bullet}$ radical cation should be, but our current work suggests it may be lower than that of TPP itself. The marked decrease in magnetic moments as a function of decreasing temperature seen in Figure 7 reveals antiferromagnetic coupling in both systems. It is qualitatively evident that spin coupling is stronger in form 1 than in the β phase. A quantitative treatment leads to the theoretical fits displayed in the same figure. Fitting parameters are given in the figure caption. The derived values of the isotropic exchange coupling parameter J (in terms of the $-2J$ spin Hamiltonian) are -54 and -15 cm^{-1} for form 1 and the β phase, respectively. From our experience with the theoretical fitting variables, the uncertainty of the precise diamagnetic correction, and the sample aging difficulties with form 1, we estimate these values are reliable to within about 10%. Particularly because of the aging problem with the dichloromethane solvate, the $|-J|$ value for form 1 should be considered a lower limit. For the purposes of the present study, the qualitatively conclusion is probably the most important one. Antiferromagnetic coupling is significantly stronger in form 1 than in the β phase, and this correlates with the relative extent of the dimer interactions seen in the crystal structures. Table VI lists the dimensional criteria discussed earlier for describing the extent of dimer interaction. Although it is too early to judge which is the most important for magnetic coupling, it seems likely that both the interplanar separation and the degree of lateral overlap are critical.

Conclusions. The apparently quite strong driving force toward pairwise association of metallotetraphenylporphyrin π-cation-radical species is further demonstrated in these studies. Dimer formation has significant effects on the molecular structure, leading to an unusual saddle-shaped core conformation. Solid-state dimer formation also leads to antiferromagnetic coupling between the ring radicals and the extent of the coupling appears to be quite sensitive to the extent of porphyrin core overlap. Since spin coupling is insufficient to produce diamagnetism at room temperature, the present work supports the partitioning of intra- and intermolecular spin coupling effects previously made in iron(III) and copper(II) porphyrin radicals.[3,4]

Acknowledgment. We thank Drs. R. H. Blessing and G. DeTitta of the Medical Foundation of Buffalo for providing us the Fortran code of the profile analysis software and Dr. P. D. W. Boyd of the University of Auckland, New Zealand, for magnetic susceptibility fitting programs. We thank Ted Brennan for work on the structure of $[Zn(TPP^{\bullet})(OH_2)]ClO_4$. We gratefully acknowledge support of this research by the National Institutes of Health (Grants GM-38401 to W.R.S. and GM-23851 to C.A.R).

Registry No. $[Zn(TPP^{\bullet})(OClO_3)]\cdot 2CH_2Cl_2$, 119946-95-1.

Supplementary Material Available: Figure S1 (an edge-on view of the dimer of form 2), Figures S2 and S3 (overlap diagrams of the porphyrin core pairs (including phenyl rings)), Figures S4 and S5 (cell-packing diagrams), Tables SI and SII (magnetic susceptibility data for form 1 and the β phase, respectively), Table SIII (complete crystallographic details), and Tables SIV and SV (thermal parameters for the atoms of $[Zn(TPP^{\bullet})(OClO_3)]$ of forms 1 and 2, respectively) (11 pages); listings of observed and calculated structure factor amplitudes (×10) for the two structures (42 pages). Ordering information is given on any current masthead page.

(29) Boudreaux, E. A.; Mulay, L. N. *Theory and Applications of Molecular Paramagnetism*; Wiley: New York, 1976.
(30) Eaton, S. S.; Eaton, G. R. *Inorg. Chem.* **1980**, *19*, 1096–1098.

Contribution from Chemistry Department A, Technical University of Denmark, DK-2800 Lyngby, Denmark, Institute of Chemical Engineering and High Temperature Processes, University of Patras, Gr-26110 Patras, Greece, and Chemistry Department B, Technical University of Denmark, DK-2800 Lyngby, Denmark

Crystal Structure and Infrared and Raman Spectra of $K_4(VO)_3(SO_4)_5$

R. Fehrmann,[1a] S. Boghosian,[1b,c] G. N. Papatheodorou,[1b,c] K. Nielsen,[1d] R. W. Berg,*[,1a] and N. J. Bjerrum[1a]

Received June 17, 1988

Blue crystals of $K_4(VO)_3(SO_4)_5$ suitable for X-ray structure determination have been obtained from solutions of V_2O_5 in molten $K_2S_2O_7$ under a SO_2/N_2 gas mixture. Lowering the temperature from the range 470–450 °C to the range 440–420 °C causes small crystals to precipitate after several hours. The compound crystallizes in the monoclinic space group $P2_1/n$ (No. 14) with $a = 8.746$ (2) Å, $b = 16.142$ (2) Å, $c = 14.416$ (2) Å, and $\beta = 106.81$ (1)° at 18 °C and $Z = 4$. It contains three different distorted VO_6 octahedra and five distorted SO_4 tetrahedra. The central vanadium atoms have a short bond to one oxide ion, four longer bonds to the oxygens of four sulfate groups, and an especially long axial bond to a fifth SO_4^{2-}. The vanadium environment is similar to what is found for other vanadyl compounds. The structure has five different sulfate groups, with three of the four sulfate oxygens bridging the vanadiums in a complicated packing pattern. Principal component analyses were performed to examine structure correlations among different sulfate and VO_6 groups. Infrared and Raman spectra of the compound have been recorded and interpreted.

Introduction

The chemistry of the molten V_2O_5–$KHSO_4$–$K_2S_2O_7$ system in contact with $SO_2/O_2/SO_3/N_2$ is being investigated due to its importance as a catalyst for the production of sulfuric acid. The investigations so far include a study[2] of the pure solvent system $KHSO_4$–$K_2S_2O_7$ and the V_2O_5–$K_2S_2O_7$–K_2SO_4 system dilute in vanadium[3] and studies[4–6] of this system at 400–500 °C, including

(1) (a) Chemistry Department A, Technical University of Denmark. (b) University of Patras. (c) Visiting Scientist at the Technical University of Denmark in 1985. (d) Chemistry Department B, Technical University of Denmark.
(2) Fehrmann, R.; Hansen, N. H.; Bjerrum, N. J. *Inorg. Chem.* **1983**, *22*, 4009.
(3) Hansen, N. H.; Fehrmann, R.; Bjerrum, N. J. *Inorg. Chem.* **1982**, *21*, 744.
(4) Fehrmann, R.; Gaune-Escard, M.; Bjerrum, N. J. *Inorg. Chem.* **1986**, *25*, 1132.

0020-1669/89/1328-1847$01.50/0

melts of the molar ratio range K/V = 2–5, corresponding to the composition of the commercial catalyst. In the V_2O_5–$K_2S_2O_7$ system, vanadium(V) at small mole fractions, $X_{V_2O_5}$, is most probably present as the monomeric oxo sulfato complexes $VO_2SO_4^-$ and $VO_2SO_4S_2O_7^{3-}$, whereas the dimeric complex $(VO_2)_2(SO_4)_2S_2O_7^{4-}$ and polymeric complexes, formulated as $(VO_2SO_4)_n^{n-}$, seem to be formed at higher mole fractions. The compounds $K_3VO_2SO_4S_2O_7$, $K_4(VO_2)_2(SO_4)_2S_2O_7$, and KVO_2SO_4 have been isolated from the melts.[7]

The formation of complexes in the molten V_2O_5–$K_2S_2O_7$ system *in contact with an SO_2 gas atmosphere* has been investigated to a much lesser extent. So far, the only paper concerning the complex formation of V(IV) in molten $K_2S_2O_7$ (at 430 °C) claims[8] a doubtful existence of the species $VOSO_4$ and $VO(SO_4)_3^{4-}$. The investigation[8] was apparently based on electrochemical measurements on $K_2S_2O_7$ melts to which "wet" chemicals like $VOSO_4 \cdot 3.5H_2O$ were added (changing the solvent to $KHSO_4$ due to the reaction $K_2S_2O_7 + H_2O \rightarrow 2KHSO_4$). Furthermore, the partial pressure of SO_2 apparently was not controlled, thus leading to an unknown conversion of V(IV) to V(V).

For a catalyst under operational conditions, it has been shown by ESR measurements[9] that V(IV) species are present both in the solid state and in solution, most probably as the (solvated) vanadyl ion, VO^{2+}. The progressive deactivation of the catalyst at temperatures below ~440 °C seems to be related to precipitation of a vanadium(IV) compound. The compound seems to be formed[10] at the expense of the solute V(IV) species in the catalyst at decreasing temperatures below ~480 °C, thus depleting the melt of active vanadium species.

Although solid compounds formed in the molten V_2O_5–$K_2S_2O_7$ system at catalyst operation conditions were examined,[11] no V(IV) compound has been isolated or identified from the working catalyst. However, melts with the molar ratio K/V = 1 and 6 were treated with a gas stream of 7.5% SO_2 (30% of SO_2 converted to SO_3), 11% O_2, and 81.5% N_2 at 420 °C. From this melt a compound, containing vanadium in the +IV oxidation state only, was observed having the composition $K_2O \cdot V_2O_4 \cdot 3SO_3$. The IR spectrum in KBr and the X-ray powder pattern resemble similar data for the stoichiometrically analogue compound $K_2SO_4 \cdot 2VOSO_4$ obtained[12] by calcination of K_2SO_4 and $VOSO_4$.

Very recently[13] we reported the structure of a V(III) compound, $KV(SO_4)_2$, isolated from the molten V_2O_5 (or V_2O_4)–$KHSO_4$–SO_2(g) system by slow stepwise decrease of the temperature from 450 to 250 °C. This gave evidence for a possible formation of vanadium compounds of oxidation states lower than +V and +IV in melts analogous to the catalyst. The present paper describes the stoichiometry and structure of a new V(IV) compound, $K_4(VO)_3(SO_4)_5$, which might be important to understanding the deactivation of the sulfuric acid catalyst.

Experimental Section

The equipment included a gas-mixing unit that was able to produce a continuous flow of any desired $SO_2/O_2/SO_3/N_2$ ratio. Details of the system will be given elsewhere.[14] The flow was introduced via stainless steel tubes to the reactor cell placed in a furnace to establish a situation that simulated a working catalyst. The furnace was a tiltable double-quartz-walled transparent tube furnace, in which the temperature of the melt could be regulated to ±0.5 °C within the range 20–500 °C. The reactor cell, made of Pyrex (Figure 1), was placed in the furnace at a position such that the bulb (B) was in the middle of the hot zone and the inlet and outlet seals were outside the furnace. A sufficiently slow gas flow passed through the inlet seal (A) and along the tube that heated the gas. Then it entered the reactor from below via a porous sintered glass-filter disk (C), bubbling through the melt (contained in the bulb B) and leaving the reactor through the outlet. This cell construction enabled us to separate precipitates on the filter disk (C) and isolate the melt filtrate in the bottom ampule (D) for separate analysis.

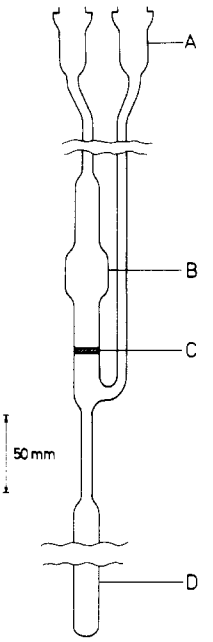

Figure 1. Reactor cell made of Pyrex for dynamic tests of catalytic melts: (A) inlet of gas flow; (B) bulb on main chamber; (C) glass-filter disk; (D) bottom ampule for filtrate.

Materials. The $K_2S_2O_7$ used was synthesized by thermal decomposition of $K_2S_2O_8$ (Merck, maximum 0.001% N) and stored in sealed ampules until used, as earlier described.[3] The nonhygroscopic V_2O_5 (Cerac, Pure (99.9%)) was used without further purification. All handling of chemicals including the filling of the reactor cell was performed in a glovebox with a nitrogen atmosphere that was continuously dried to around 5 ppm H_2O by means of circulation through a column with molecular sieves. Commercial gases in steel bottles were used: SO_2 (>99.9%), O_2 (99.8% O_2 + 0.2% N_2 and Ar), and N_2 (<40 ppm O_2 + H_2O).

Synthesis of Crystalline $K_4(VO)_3(SO_4)_5$. In the glovebox, $K_2S_2O_7$ and V_2O_5 were added to the reactor cell (Figure 1) at molar ratios K/V = 3, 4, or 10. Usually the volume of the components did not exceed 1.5 mL (when fused) to avoid excessive foaming, which might stop the gas flow by solidification of the melt in the cold part of the tube leading out of the reactor. The cell was transferred in closed condition to the reactor furnace and quickly connected to the gas supply and vent tubes. After being heated to 430–470 °C (well above the melting points of the mixtures), $SO_2/O_2/SO_3/N_2$ gas mixtures of the desired composition were gently bubbled through the melt, at a total flow of around 2 mL/min. When the gas consisted of SO_2/N_2 mixtures or SO_2 only, green and blue precipitates were observed after equilibration overnight. Large crops of crystals were obtained at low temperatures, i.e. in the range 440–420 °C and especially at $pSO_2 \geq 0.1$ atm. A thorough study is in progress on the influence of various parameters on precipitation, including the composition of the melt, the composition of the gas mixture, and the temperature. After cooling, the reactor cell was opened and flushed gently with water overnight to dissolve the crystallized $K_2S_2O_7$ solvent. In this way, very slightly soluble bright blue crystals and sometimes also green hexagonal crystals remained.

Similar blue and green compounds were also obtained from melts equilibrated in Pyrex ampules sealed under a SO_2 pressure of about 0.9

(5) Hatem, G.; Fehrmann, R.; Gaune-Escard, M.; Bjerrum, N. J. *J. Phys. Chem.* **1987**, *91*, 195.
(6) Hatem, G.; Fehrmann, R.; Gaune-Escard, M.; Bjerrum, N. J. To be submitted for publication.
(7) Glazyrin, M. P.; Krasil'nikov, V. N.; Ivakin, A. A. *Russ. J. Inorg. Chem. (Engl. Transl.)* **1980**, *25*, 1843; **1982**, *27*, 1740.
(8) Durand, A.; Picard, G.; Vedel, J. *J. Electroanal. Chem. Interfacial Electrochem.* **1981**, *127*, 169.
(9) Boreskov, G. K.; Davydova, L. P.; Mastikhin, V. M.; Polyakova, G. M. *Dokl. Akad. Nauk SSSR* **1966**, *171*, 648; *Dokl. Chem. (Engl. Transl.)* **1966**, *171*, 760.
(10) Mastikhin, V. M.; Polyakova, G. M.; Zyulkovskii, Y.; Boreskov, G. K. *Kinet. Katal.* **1970**, *11*, 1463; *Kinet. Catal. (Engl. Transl.)* **1970**, *11*, 1219.
(11) Bazarova, Z. G.; Boreskov, G. K.; Ivanov, A. A.; Karakchiev, L. G.; Kacohkina, L. D. *Kinet. Katal.* **1971**, *12*, 948; *Kinet. Catal. (Engl. Transl.)* **1971**, *12*, 845.
(12) Ezhkova, Z. I.; Zaitsev, B. E.; Konysheva, L. I.; Matveevicheva, V. A.; Nekhorosheva, N. I.; Polotnyuk, O.-V. Y.; Chaikovskii, S. P. *Kinet. Katal.* **1972**, *13*, 1288; *Kinet. Catal. (Engl. Transl.)* **1972**, *13*, 1149.
(13) Fehrmann, R.; Krebs, B.; Papatheodorou, G. N.; Berg, R. W.; Bjerrum, N. J. *Inorg. Chem.* **1986**, *25*, 1571.
(14) Boghosian, S.; Fehrmann, R.; Bjerrum, N. J.; Papatheodorou, G. N. *J. Catal.*, in press.

Table I. Crystallographic Data for Potassium Vanadyl Sulfate

$K_4(VO)_3(SO_4)_5$	fw 837.54
a = 8.746 (2) Å	space group $P2_1/n$ (No. 14)
b = 16.142 (2) Å	T = 18 °C
c = 14.416 (2) Å	λ = 0.71069 Å (Mo Kα)
β = 106.81 (1)°	μ = 29.6 cm^{-1}
V = 1948.25 Å^3	abs cor: none
Z = 4 formula units/cell	$R(F_o)$ = 0.030
ρ_{exp} = 2.87 g cm^{-3}	$R_w(F_o^2)$ = 0.042
ρ_{calcd} = 2.85 g cm^{-3}	

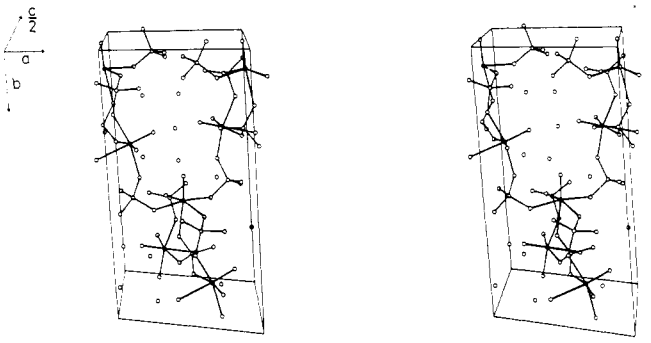

Figure 2. Stereoview of a fraction ($\geq 1/2$) of the unit cell of $K_4(VO)_3(SO_4)_5$.

atm at room temperature. It seemed that the blue compound preferentially precipitated when the melts were equilibrated at lower temperatures and low partial pressures of SO_2 whereas increasing amounts of the green compound were seen with increasing temperature and pressure of SO_2 (details will be given elsewhere[14]). The green compound was presumably the vanadium(III) compound, $KV(SO_4)_2$, previously isolated from similar melts.[13]

The blue crystals were examined in a polarization microscope (habit: irregular short rods or thick plates), and proper samples were selected for further investigation.

Chemical analyses by atomic absorption and flame emission spectrometry with respect to V and K were in close accordance with the formula $K_4(VO)_3(SO_4)_5$ (Anal. Calcd: K, 18.68; V, 18.25. Found: K, 18.8 ± 0.7; V, 18.1 ± 0.4. Standard substances K_2SO_4 and V_2O_5, pro analysi).

Infrared Spectra. The IR spectra were recorded on a Perkin-Elmer 297 spectrometer in double-beam mode with a KBr disk as the reference.

Raman Spectra. For recording of the Raman spectra, the excitation wavelengths of 488.0 and 514.5 nm of an argon ion laser were used, giving essentially identical spectra, although small changes in relative intensities were observed. The power level needed to be reduced to ~100 mW to avoid decomposition of the sample.

The scattered light was collected at an angle of 90° and sent through a 90° image rotator and a polarization scrambler, the entrance slit being vertical and the scattering plane horizontal. A JEOL JRS-400D 0.4-m double monochromator and a cooled S-20 photomultiplier with photon counting were applied and calibrated with a neon discharge lamp.

X-ray Investigation

Determination of the Crystal Structure. Intensity data were collected at 18 °C on an Enraf-Nonius CAD-4F diffractometer. The cell dimensions were determined by least-squares refinement based on the setting of 25 high-order reflections. The crystal structure was solved by direct methods.[15] The remaining atoms was found by Fourier techniques, and the structural parameters was refined by block diagonal least-squares methods.[16] The very irregular shape of the crystal was suspected to produce unreliable corrections for absorption and extinction; consequently, no corrections were attempted. Instead, the deficiencies of the model was compensated for by designing the weight function to give as uniform a distribution of $w|\Delta F|^2$ as possible.[17] As a result, the six strongest reflections, apart from those with $I < 2\sigma(I)$, were omitted from the refinement. Crystal data and details on data collection and refinement of the structure are given in Table I. The final positional parameters are listed in Table II. Figure 2 shows a stereopair of the structure. Tables A and B of thermal parameters and observed and calculated structure factors are available as supplementary material.

Comparison of Crystallographically Independent Groups. The asymmetric unit contains three independent VO_6 octahedra and five independent SO_4 tetrahedra. In order to simplify the com-

Table II. Coordinates of the Atoms in the $K_4(VO)_3(SO_4)_5$ Structure[a]

atom	x	y	z
V(1)	0.164 56 (4)	0.358 93 (2)	0.087 93 (2)
V(2)	−0.008 42 (3)	0.109 00 (2)	0.253 53 (2)
V(3)	0.321 76 (4)	0.138 77 (2)	−0.080 11 (2)
S(1)	0.098 15 (5)	0.155 50 (3)	0.059 57 (3)
S(2)	0.453 71 (5)	0.178 15 (3)	−0.264 22 (3)
S(3)	−0.121 47 (5)	0.161 30 (3)	0.443 91 (3)
S(4)	0.839 75 (5)	0.562 60 (3)	0.398 99 (3)
S(5)	0.840 85 (5)	0.435 44 (3)	0.899 17 (3)
K(1)	0.739 80 (5)	0.246 64 (3)	0.985 20 (4)
K(2)	−0.252 09 (6)	−0.022 58 (3)	0.378 67 (4)
K(3)	0.021 61 (8)	0.300 88 (4)	0.737 49 (5)
K(4)	0.220 81 (6)	0.473 99 (3)	0.358 03 (4)
O(1)	0.348 98 (18)	0.359 57 (10)	0.839 30 (10)
O(2)	0.620 52 (18)	0.380 50 (9)	0.657 69 (10)
O(3)	0.539 42 (19)	0.255 57 (9)	0.766 82 (11)
O(4)	0.770 29 (17)	0.483 94 (8)	0.421 63 (11)
O(5)	0.560 45 (17)	0.254 97 (9)	0.561 26 (11)
O(6)	0.717 02 (18)	0.018 57 (9)	0.582 63 (11)
O(7)	0.498 95 (19)	0.391 09 (10)	0.004 54 (12)
O(8)	0.550 34 (19)	0.123 43 (9)	0.690 41 (10)
O(9)	0.428 13 (17)	0.250 77 (9)	0.959 47 (11)
O(10)	0.472 25 (19)	0.384 61 (10)	0.486 62 (11)
O(11)	0.219 81 (17)	0.348 85 (9)	0.960 45 (10)
O(12)	0.448 64 (19)	0.129 67 (9)	0.822 76 (11)
O(13)	0.292 31 (16)	0.376 73 (8)	0.640 77 (10)
O(14)	0.480 31 (20)	0.488 78 (10)	0.761 54 (11)
O(15)	0.699 01 (17)	0.380 83 (8)	0.861 58 (10)
O(16)	0.758 34 (17)	0.355 23 (9)	0.544 59 (10)
O(17)	0.659 81 (19)	0.329 62 (10)	0.347 74 (12)
O(18)	0.329 96 (19)	0.329 58 (10)	0.158 90 (12)
O(19)	0.928 34 (17)	0.398 61 (9)	0.993 27 (10)
O(20)	0.934 66 (19)	0.439 61 (10)	0.831 39 (11)
O(21)	0.063 89 (18)	0.400 61 (10)	0.509 28 (11)
O(22)	0.070 18 (20)	0.450 04 (10)	0.669 65 (12)
O(23)	0.295 06 (18)	0.190 14 (10)	0.670 87 (11)

[a] The temperature factor parameters are given in the supplementary material.

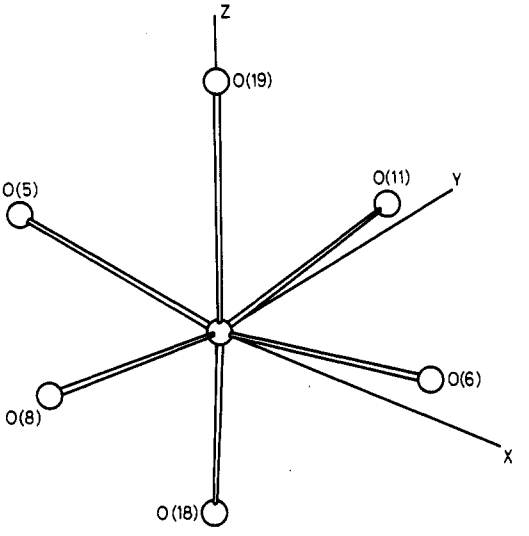

Figure 3. Definition of the local coordinate system for the VO_6 units. The longest V–O bond lies along z, and one oxygen lies in the yz plane. Oxygen atoms in the V(1) octahedron are shown. For the corresponding atoms in V(2) and V(3) octahedra, see Table III.

(15) Germain, G.; Main, P.; Woolfson, M. *Acta Crystallogr.* **1971**, *A27*, 368.
(16) Stewart, J. M.; Kundell, F. A.; Baldwin, J. C. "The X-ray System, Version of 1972"; Technical Report TR-192; Computer Science Center, University of Maryland: College Park, MD, 1972.
(17) Nielsen, K. *Acta Crystallogr.* **1977**, *A33*, 1009.
(18) *International Tables for X-Ray Crystallography*; Kynoch Press: Birmingham, England, 1974; Vol. IV.

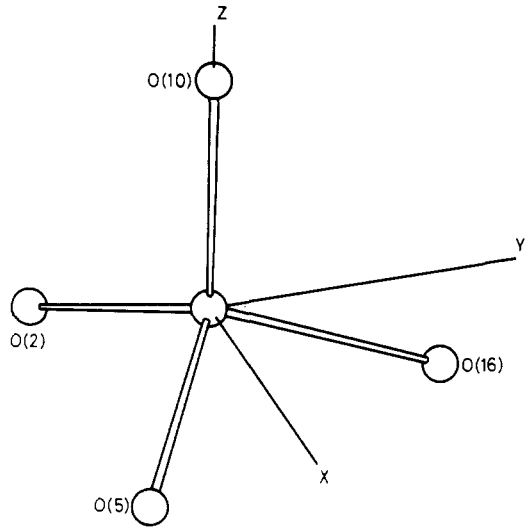

Figure 4. Definition of the local coordinate system for the SO_4 groups. The shortest S–O bond lies along z, and one oxygen atom is fixed to the yz plane. Oxygen atoms in the S(1) tetrahedron are shown. For the corresponding atoms in S(2)–S(5) tetrahedra, see Table III.

Table III. Ordering of the Oxygen Atoms for the Three VO_6 Units and the Five SO_4 Units[a]

central atom	coordinated atoms: axial short	axial long	equatorial			
V(1)	O(18)	O(19)	O(11)	O(5)	O(6)	O(8)
V(2)	O(14)	O(3)	O(13)	O(2)	O(1)	O(15)
V(3)	O(17)	O(21)	O(16)	O(9)	O(4)	O(12)

central atom	coordinated atoms			
S(1)	O(10)	O(16) e	O(2) e	O(5) e
S(2)	O(23)	O(12) e	O(8) e	O(3) a
S(3)	O(7)	O(11) e	O(1) e	O(9) e
S(4)	O(22)	O(21) a	O(13) e	O(4) e
S(5)	O(20)	O(19) a	O(15) e	O(6) e

[a] Each column lists equivalent oxygen atoms[b] as determined by least-squares methods. A letter a or e indicates that the oxygen atom is axially or equatorially bonded to V.[c] [b] For the meaning of equivalent, see text. [c] The axis is defined by the short V–O bond.

parison of independent groups, the following procedure was adopted. The coordinates of each group were transformed into a local orthogonal coordinate system. The central atom (vanadium or sulfur) was placed at the origin, one atom was placed on the z axis, and one in the yz plane. Schematic drawings of the coordinate system for the VO_6 units and the SO_4 units are shown in Figures 3 and 4. One group is kept fixed, and the remaining groups of the same kind were rotated and translated in order to minimize the discrepancies in the coordinates. The quantity minimized was

$$\sum_i \sum_j \sum_n w_{ijn}(X_{in} - X_{jn})^2 \qquad (1)$$

where X_{in} is the nth coordinate in the ith group and w is a weight inversely proportional to the sum of the variance of the two coordinates in question. The number of ways (including inversion symmetry) in which we allowed groups to be oriented in the local coordinate system was reduced by inspection of the distances and angles. Totally, this gave 64 allowed configurations for the VO_6 octahedra and 192 for the sulfate groups, and each of these configurations was subjected to rotations and translations in order to minimize eq 1. The configuration leading to an absolute minimum of eq 1 then produced an ordering of the oxygen atoms (Table III). In the following, the VO_6 or SO_4 units will be designated Vi or Si (i = integer) in accordance with the V(i) or S(i) labeling of the central atoms. Thus, in Tables IV and V, bond distances or bond angles for the VO_6 and SO_4 groups are listed,

Table IV. V–O Distances (Å) and O–V–O Angles (deg)[a]

	V1	V2	V3
	Bonds[b]		
V–O(18)	1.584 (2)	1.588 (2)	1.580 (2)
V–O(19)	2.216 (1)	2.224 (2)	2.230 (2)
V–O(11)	2.038 (2)	2.023 (1)	2.031 (2)
V–O(5)	2.038 (1)	2.028 (2)	2.038 (1)
V–O(8)	2.029 (2)	2.027 (1)	2.028 (2)
V–O(6)	2.036 (2)	2.058 (2)	2.033 (1)
	Angles		
O(18)–V–O(19)	177.6 (3)	170.1	173.4 (2)
O(18)–V–O(11)	98.5	96.6	98.3
O(18)–V–O(5)	97.3	101.0	98.5
O(18)–V–O(8)	97.0	94.9	97.7
O(18)–V–O(6)	98.1	98.1	99.4
O(19)–V–O(11)	83.7	93.1	87.6
O(19)–V–O(5)	81.9	81.3	79.1
O(19)–V–O(8)	80.8	75.5	76.1
O(19)–V–O(6)	82.9	80.6	83.8
O(11)–V–O(5)	88.1	87.9	85.9
O(11)–V–O(8)	164.4	168.4	163.5
O(11)–V–O(6)	85.9	85.6	85.3
O(5)–V–O(8)	88.7	88.1	87.8
O(5)–V–O(6)	164.2	160.4	161.0
O(8)–V–O(6)	93.1	94.7	96.0

[a] For distances, estimated standard deviations are always given; for angles, they are only given when larger than 0.1°. [b] Oxygens specified are the bonds around V1, in column 2. For bonds of V2 and V3 (columns 3 and 4), one should consult Table III to find the appropriate oxygens.

Table V. S–O Distances (Å) and O–S–O Angles (deg)[a]

	S1	S2	S3	S4	S5
	Bonds[b]				
S–O(10)	1.438	1.445	1.434	1.446	1.448
S–O(16)	1.488	1.490	1.484	1.472	1.476
S–O(2)	1.489	1.497	1.493	1.496	1.490
S–O(5)	1.484	1.459	1.482	1.484	1.484
	Angles				
O(10)–S–O(16)	113.3	111.0	113.2	112.8	113.2
O(10)–S–O(2)	112.4	110.7	111.4	110.1	110.9
O(10)–S–O(5)	108.9	113.3	110.0	111.6	111.5
O(16)–S–O(2)	102.8	102.5	103.9	105.0	104.6
O(16)–S–O(5)	109.8	109.2	109.1	108.2	108.3
O(2)–S–O(5)	109.5	109.5	109.1	108.9	108.0

[a] For distances and angles, the standard deviations are ≤0.002 Å and 0.1°, respectively. [b] Oxygens specified are the bonds around S1, in column 2. For S2–S5 (columns 3–6), one should consult Table III to find the appropriate oxygens.

oxygen atoms being specified with respect to V1 or S1 (first column). The remaining distances or angles (next columns) involve other oxygen atoms, whose numbers may be found by consulting Table III.

Principal Component Analysis, PCA. The refined orthogonal coordinates, X_{in}, were used for PCA.[19] Each group was assigned a weight, w_n, inversely proportional to the average variance of the coordinates in the group. The proportionality constant was determined such that $\sum w_n = 1$. The average coordinates among all groups of V or S were calculated and subtracted from the coordinates in each group. On the basis of D_{ni}, the deviation from average of the ith coordinate in the nth group, a matrix **M**, with elements $M_{ij} = \sum w_n D_{ni} D_{nj}$ was calculated. M_{ii}, the ith diagonal element of **M**, is equal to the total squared deviation of the ith coordinate, and the trace, R, of **M** is the total squared deviation. R is invariant to any unitary transformation of **M**. When the eigenvalue problem, **MU** = **UΛ**, is solved, the total squared deviation (R) concentrates in as few diagonal elements as possible.[19]

(19) Wold, S.; et al. In *Chemometrics, Mathematics and Statistics in Chemistry*; Kowalsky, B. R., Ed.; Reidel: Dordrecht, The Netherlands, 1984; p 17. Murray-Rust, P.; Bland, R. *Acta Crystallogr.* **1978**, *B34*, 2527.

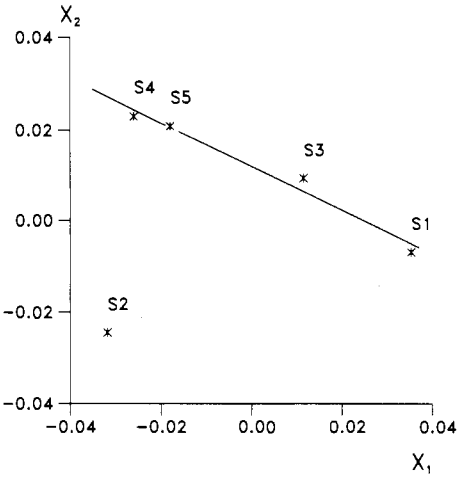

Figure 5. Correlation between the two major transformed parameters X_1 and X_2 for the five sulfate groups.

Λ is a diagonal matrix containing the eigenvalues, and **U** contains the eigenvectors. To each eigenvalue there corresponds a new set of deviations, $X_{ni} = \sum_j D_{nj}U_{ji}$, which, provided the eigenvalues are ordered in a decreasing sequence, will be of decreasing importance in the description of the geometry of the groups. A PCA provides the opportunity of describing differences between the groups by few parameters. With m parameters the description accounts for $100\sum_{i=1}^{m}\Lambda_{ii}/R$ (%) of the total squared deviation, and furthermore, it is the highest possible fraction that can be accounted for by any description with m parameters.

Geometry of the Sulfate Groups. In each of the five sulfate groups, three of the oxygen atoms are coordinated to three different vanadium atoms. Of these 15 bridging oxygen atoms, three are *axially* coordinated to vanadium, i.e. opposite to the V=O bond. This results in a longer V–O bond, which is compensated for by a shorter S–O bond. The three axially coordinated oxygen atoms are distributed among sulfate groups S2, S4, and S5. The axially coordinated oxygen atoms for S4 and S5 are in a least-square sense equivalent to O(16), and the corresponding oxygen atom for S2 is equivalent to O(5). With the five sulfate groups, the PCA resulted in at most four nonzero eigenvalues. The value of R is 1.105×10^{-3}, and the two major eigenvalues account for 96.4% of R. Thus, to a very large extent the geometrical differences between the sulfate groups can be described by two parameters. As seen from Figure 5, S2 seems to be different from the four other groups, for which the two major parameters are almost linearly related. This means that the geometrical differences between these four groups can be depicted by one parameter and that a second parameter must be used to include S2 in the description of the deviations. A subsequent PCA on S1, S3, S4, and S5 gave as result that 95.8% of R can be accounted for by a single parameter. The major geometrical difference is a shift in the z coordinate of O(2) and a shift in the opposite direction of the z coordinate of O(5). As expected, the S–O(2) and S–O(5) distances only show small fluctuations. The largest differences are found in the O–S–O angles involving O(2) and O(5). That the transformed deviation describes the angular fluctuations is confirmed by the high correlation between the new deviation and the O(10)–S–O(2), O(10)–S–O(5), O(16)–S–O(2), and O(16)–S–O(5) angles. The values of the correlation coefficients are 0.968, −0.977, −0.993, and 0.999, respectively.

The O–S–O angles for which both oxygen atoms are coordinated to vanadium can be correlated to the geometrical arrangement of the V–O–S–O–V chain. Two different types of arrangement are found in the structure, and examples are shown in Figure 6. In one type of arrangement, found once per sulfate group, the V–V distances range from 6.213 to 6.461 Å, and the oxygen atoms lie close (within 0.6 Å) to the V–V line. The corresponding O–S–O angle is less than 105°. Of the five V–O–S–O–V chains, the two with the longest V–V distances involve axially coordinated oxygen atoms (in groups S4 and S5). The other type of arrangement comprises O–S–O angles larger than

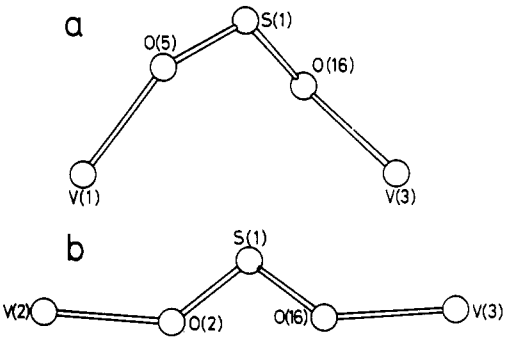

Figure 6. The two different types of geometrical arrangements found for the V–O–S–O–V chains: (a) arrangement corresponds to an O–S–O angle larger than 108°; (b) arrangement corresponds to an O–S–O angle less than 105°.

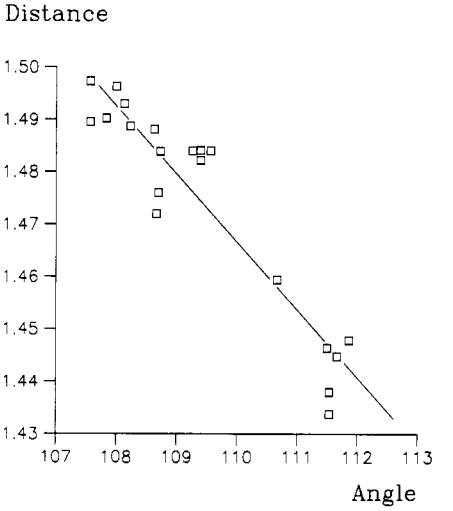

Figure 7. Plot of S–O distances versus the average of the O–S–O angles involving the bond. A regression line is shown.

108°. The V–V distances are shorter (4.724–5.157 Å), and the oxygen atoms lie more distant from the V–V line (~1.5 Å). Consequently, for the two different types of arrangement, sulfur atoms lie more or less distant from the V–V line. There is a reasonable correlation between the O–S–O angle and this distance (correlation coefficient is 0.984). In conclusion, it indicates that the low O–S–O angle is a consequence of the packing forces.

This result, as well as the results from the least-squares analysis and the PCA, show that the major differences in the geometry of the sulfate groups are closely correlated to differences in the O–S–O angles. It should therefore be expected that the S–O distances fluctuate an order of magnitude, explanable by changes in the hybridization of the sulfur atom. Within the model of an sp^3-hybridized sulfur atom with the four hybrid orbitals directed toward the oxygen atoms, it can be expected that the higher the s character of the bond, the shorter the bond. Unfortunately, it is not possible to establish the s character of an S–O bond for the general tetrahedral case.[20] However, if the fluctuations in the distances depend on the differences in hybridization, the S–O distance should be almost linearly correlated to the O–S–O angles involving the bond. Figure 7 depicts the S–O distance as a function of the average of the three angles involving the bond. The trend in the curve seems clear: Within this crude model, which also excludes the effect of differences in the hybridization of the oxygen atoms, there is an approximate linear relationship between angles and distances.

Geometry of the VO_6 Groups. For the three VO_6 groups, the PCA resulted in at most two nonzero eigenvalues. The value of R is 1.554×10^{-2}, and the parameter corresponding to the largest eigenvalue accounts for 83.3% of R. A fairly good description

(20) Coulson, C. A. In *Victor Henry Memorial Volume, Contribution to the Study of Molecular Structure*; Maison Desoer: Liege, Belgium, 1948.

Table VI. Distances (Å) between an Atom and Its Symmetry-Transformed Counterpart in $C2/c$

atoms	dist	site sym[a]	atoms	dist	site sym[a]
V(1)–V(3)[b]	0.190		O(5)–O(9)	0.348	
V(2)[c]	0.202	2	O(7)–O(10)	0.268	
S(1)–S(3)	0.242		O(8)–O(12)	0.217	
S(4)–S(5)	0.033		O(11)–O(16)	0.246	
S(2)	0.795	2	O(13)–O(15)	0.113	
K(2)–K(4)	0.327		O(14)	0.544	2
K(1)	0.426	$\bar{1}$	O(17)–O(18)	0.149	
K(3)	0.593	2	O(19)–O(21)	0.092	
O(1)–O(2)	0.425		O(20)–O(22)	0.173	
O(3)	0.719	2	O(23)		
O(4)–O(6)	0.147				

[a] Site symmetry is given if different from 1. [b] E.g., the $C2/c$ symmetry operation $(1/2 - x, 1/2 - y, -z)$ transforms V(3) to a position (0.17823, 0.36123, 0.08011) that is 0.190 Å removed from V(1). [c] E.g., the $C2/c$ symmetry operation $(-x, y, 1/2 - z)$ transforms V(2) to a position (−0.00842, 0.10900, 0.24647) that is 0.202 Å removed from V(2).

of the differences between the VO_6 groups can be obtained by a single parameter. The major changes are shifts in the y coordinate of O(19) and the z coordinate of O(11), changes that primarily affect angles not involving O(5) and O(6).

Approximate Description of the Structure in Space Group $C2/c$. The hypothesis that differences in the geometry of the sulfate ions are a consequence of differences in packing is supported by an approximate description of the structure in $C2/c$. An inspection of the atomic coordinates (in Table II) shows that the structure is approximately C-centered, changing the space group from $P2_1/n$ to $C2/c$. These extra approximate symmetry elements will pair atoms and groups without site symmetry in $C2/c$: S1 with S3, S4 with S5, and V1 with V3. The ordering of the oxygen atoms produced by pairing is in agreement with that obtained by the least-squares analyses. S2 and V2 have their central atoms placed on the approximate 2-fold axis. The pairing of the sulfate groups qualitatively agrees with the result of the PCA (Figure 5). Table VI lists the distances between an atom and its symmetry-transformed counterpart in $C2/c$. The smallest deviations from $C2/c$ symmetry are found for the (S4, S5) pair. The (S1, S3) pair has somewhat larger deviations, whereas one atom, O(23), from the S2 group does not fit into $C2/c$. It can be concluded that the (S4, S5) groups, as well as the (S1, S3) groups, have similar surroundings, surroundings that differ from those of S2. This result is in perfect agreement with the results of the PCA. In Figure 5 the distance between the S4 and S5 groups is somewhat smaller than the distance between the S1 and S3 groups, and the point for S2 lies far from the least-squares line. With O(23) omitted and with the remaining atoms placed on their average position in $C2/c$, distances and angles were recalculated. Only minor changes were observed for all groups except S2. For S2, the original configuration was markedly deformed, especially the S(2)–O(3) distance (~1.25 Å) and the angles involving O(3) (~126°).

Comparison of $K_4(VO)_3(SO_4)_5$ to Some Other Structures. The coordination around the vanadium atoms can be compared with other known V(IV) structures, particularly the other vanadyl sulfates α-$VOSO_4$,[21,22] β-$VOSO_4$,[23] $VOSO_4 \cdot 3H_2O$,[24] and $VOSO_4 \cdot 5H_2O$.[25] In these compounds, vanadium–oxygen ion pairs connected with a short (~1.56–1.61 Å) bond constitute the "vanadyl group" characteristic of V(IV) compounds.[26] Around vanadium opposite of the short V=O bond there is typically a long one (ca. 2.2–2.5 Å), the (distorted) VO_6 octahedron being completed by four equivalent V—O bonds of ca. 1.98–2.08 Å length, forming O=V—O angles of around 94–103°. By comparing this to our results in Table IV, we see that $K_4(VO)_3(SO_4)_5$ has a quite normal behavior, only the long V—O bonds opposite of V=O are as short or shorter than ever observed.

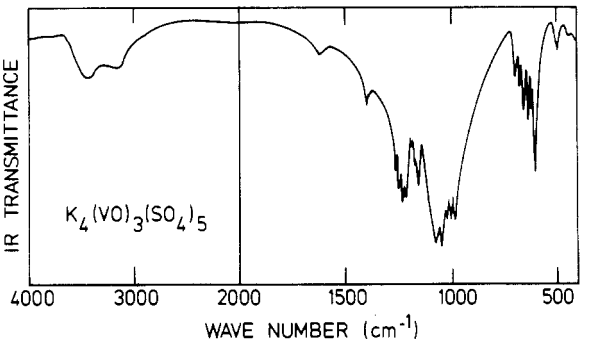

Figure 8. Infrared spectrum of $K_4(VO)_3(SO_4)_5$ powder in a pressed KBr disk at room temperature (resolution ~5 cm^{-1}).

The sulfate group S–O bond length, reported for these sulfate vanadyl structures in the literature[21-25] (ranging within 1.41–1.50 Å) are generally shorter than the 1.49 Å known from "average" sulfate structures.[27] Also, for the sulfate groups in $K_4(VO)_3(SO_4)_5$, S–O bond lengths range within previously observed limits.

Vibrational Spectra

General Considerations. Oriented single-crystal vibrational spectroscopy using polarized light is difficult to interpret when the unit cell is monoclinic and large. Therefore, only powder work is reported.

If the crystal is considered to be made from K^+, VO^{2+}, and SO_4^{2-} ions, one should expect approximately to see free group vibrations of the complex ions (here VO^{2+} and SO_4^{2-}), i.e. a number of observable ν(V=O) stretching bands (near 1000 cm^{-1})[26,28] and bands near the positions of the four fundamentals (ν_1–ν_4) of the SO_4^{2-} ion. These are well-known,[29] mainly from Raman spectroscopy on aqueous sulfate solutions:

$$\nu_1(A_1) \simeq 981 \text{ cm}^{-1}$$

$$\nu_2(E) \simeq 451 \text{ cm}^{-1}$$

$$\nu_3(F_2) \simeq 1104 \text{ cm}^{-1}$$

$$\nu_4(F_2) \simeq 613 \text{ cm}^{-1}$$

All of these are Raman-active, only F_2 species being IR allowed.

The close approach of ions and the low symmetry within the crystal are expected to shift the fundamentals moderately and to split degeneracies, but it should still be possible to identify the stretchings (ν_1 and ν_3) and the bendings (ν_2 and ν_4). Many examples of vibrational analyses of sulfates are described in recent literature, e.g. for K_2SO_4,[30-33] and also melts have been carefully studied.[34,35]

Among vanadyl sulfates previously studied by IR spectroscopy are $VOSO_4$,[12,36] mixtures of K_2SO_4 and $VOSO_4$ such as $K_2SO_4 \cdot 2VOSO_4$,[12] $K_2O \cdot V_2O_4 \cdot 3SO_3$,[11] $K_2[V_2O_2(SO_4)_3]$, and $K_2[VO(SO_4)_2]$.[37] No Raman work has been found on compounds containing vanadyl and sulfate.

(21) Ladwig, G. *Z. Anorg. Allg. Chem.* **1969**, *364*, 225.
(22) Longo, J. M.; Arnott, R. J. *Acta Crystallogr.* **1969**, *A25*, 118; *J. Solid State Chem.* **1970**, *1*, 394.
(23) Kierkegaard, P.; Longo, J. M. *Acta Chem. Scand.* **1965**, *19*, 1906.
(24) Théobald, F.; Galy, J. *Acta Crystallogr.* **1973**, *B29*, 2732.
(25) Ballhausen, C. J.; Djurinskij, B. F.; Watson, K. J. *J. Am. Chem. Soc.* **1968**, *90*, 3305.
(26) Selbin, J. *Coord. Chem. Rev.* **1966**, *1*, 293; *Chem. Rev.* **1965**, *65*, 153.
(27) McGinnety, J. A. *Acta Crystallogr.* **1972**, *B28*, 2845.
(28) Evans, J. C. *Inorg. Chem.* **1963**, *2*, 372.
(29) Nakamoto, K. *Infrared and Raman Spectra of Inorganic Coordination Compounds*; Wiley: New York, 1978.
(30) Montero, S.; Schmölz, R.; Haussühl, S. *J. Raman Spectrosc.* **1974**, *2*, 101.
(31) Meserole, F.; Decius, J. C.; Carlson, R. E. *Spectrochim. Acta, Part A* **1974**, *30A*, 2179.
(32) Brooker, M. H. *Appl. Spectrosc.* **1975**, *29*, 528.
(33) Wu, G.-J.; Frech, R. *J. Chem. Phys.* **1976**, *64*, 4897.
(34) Smith, D. H.; Begun, G. M.; Child, W. C., Jr. *J. Chem. Soc., Faraday Trans. 2* **1981**, *77*, 1399.
(35) Child, W. C., Jr.; Begun, G. M.; Smith, D. H. *J. Chem. Soc., Faraday Trans. 2* **1981**, *77*, 2237.
(36) Tudo, J. *Rev. Chim. Miner.* **1965**, *2*, 53.
(37) Krasil'nikov, V. N.; Glazyrin, M. P.; Ivakin, A. A. *Russ. J. Inorg. Chem. (Engl. Transl.)* **1983**, *28*, 1197.

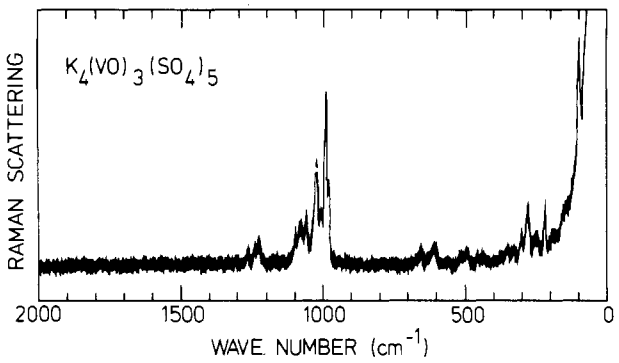

Figure 9. Raman spectra of $K_4(VO)_3(SO_4)_5$ powder at room temperature ($\lambda_0 \sim 488.0$ nm; power ~ 100 mW; resolution ~ 2 cm^{-1}).

Infrared Spectra. IR spectra of blue $K_4(VO)_3(SO_4)_5$ at room temperature (see Figure 8) were obtained on finely ground powders in pressed KBr disks. The IR band positions and tentative assignments are given in the supplementary material. The characteristic V=O stretching[26] at ca. 975 cm^{-1} on top of the presence of many bands in the sulfate stretching region (ca. 1200-1000 cm^{-1}) and the complete absence of bands[2] that might be due to $S_2O_7^{2-}$ should be noted.

Raman Spectra. Raman spectra were obtained at room temperature on stationary polycrystalline samples (Figure 9); the bands observed are listed and tentative assignments are given in the supplementary material (Table C).

Discussion. As can be seen from Figures 8 and 9, the IR and Raman spectra contain many bands and most of them are common to both kinds of spectra. This is in accordance with what is to be expected from a unit cell containing as many as three VO and five SO_4 groups in a low symmetry. Sulfate groups under various crystal environments were recently studied, and similar band-rich spectra were seen.[38] In infrared spectra of V(IV) compounds in analogous frozen-melt systems, similar features have been observed.[11,12,37] Probably, blue V(IV) compounds were formed in these SO_2-reduced systems, but the procedures of freezing the melts did not permit an isolation of pure samples, e.g. of $K_4(VO)_3(SO_4)_5$.

Conclusion

The compound $K_4(VO)_3(SO_4)_5$ has been isolated from $V_2O_5/K_2S_2O_7/SO_2$ melts, and its molecular structure was determined.

The deactivation of sulfuric acid catalysts at lower temperatures has been attributed[9,10,39,40] to the precipitation of V(IV) compounds. Furthermore, work in progress[14] shows that the compound $K_4(VO)_3(SO_4)_5$ is formed in the $V_2O_5/K_2S_2O_7$-$SO_2/O_2/N_2$ liquid-gas system, and simultaneously, a dramatic decrease in the catalytic activity of the system is seen. Thus, the precipitation of the V(IV) compound $K_4(VO)_3(SO_4)_5$ may account for the observed deactivation of the commercial catalyst at low temperatures.

Acknowledgment. This investigation was in part supported by the "Stimulation Actions" program of the European Economic Community (EEC Contract No. STI-011-J-C(CD)).

Supplementary Material Available: Tables A, C, and D, listing temperature factor parameters, IR and Raman bands, and all crystallographic data (4 pages); Table B, listing observed and calculated structure factors (31 pages). Ordering information is given on any current masthead page.

(38) Bremard, C.; Laureyns, J.; Abraham, F. *J. Raman Spectrosc.* **1986**, *17*, 397.
(39) Kozyrev, S. V.; Balzhinimaev, B. S.; Boreskov, G. K.; Ivanov, A. A.; Mastikhin, V. M. *React. Kinet. Catal. Lett.* **1982**, *20*, 53.
(40) Borisov, V. M.; Berezkina, L. G.; Bel'skaya, N. P.; Gubareva, V. N.; Petrovskaya, G. I.; Pogodilova, E. G.; Stul', R. M. *Zh. Prikl. Khimii (Leningrad)* **1987**, *60*, 612. *J. Appl. Chem. USSR (Engl. Transl.)* **1987**, *60*, 575.

Contribution from the School of Chemistry,
University of New South Wales, Kensington, NSW 2033, Australia

Monocyclic Copper and Silver Tertiary Alkanethiolates: Formation and Molecular Structures of $(CuSBu^t)_4(Ph_3P)_2$, $(AgSCMeEt_2)_8(Ph_3P)_2$, and $(AgSBu^t)_{14}(Ph_3P)_4$ and Structural Principles

Ian G. Dance,* Lyn J. Fitzpatrick, Donald C. Craig, and Marcia L. Scudder

Received August 19, 1988

The molecular compounds $(CuSBu^t)_4(Ph_3P)_2$ (**8**), $(AgSCMeEt_2)_8(Ph_3P)_2$ (**9**), and $(AgSBu^t)_{14}(Ph_3P)_4(CHCl_3)_2$ (**10**), formed by reactions of the nonmolecular metal tertiary alkanethiolates with triphenylphosphine, have been characterized by crystal structure determinations. The single cycle in **8** contains alternating segments of linear $(\mu\text{-SR})Cu^{dig}(\mu\text{-SR})$ and trigonal $(\mu\text{-SR})_2Cu^{trig}(PPh_3)$. **9** contains two different tetrasilver cycles, one $((\mu\text{-SCMeEt})_4(Ag^{dig})_4)$ with digonal silver only, and the other $((\mu\text{-SCMeEt}_2)_4(Ag^{dig})_2(Ph_3PAg^{trig})_2)$ with Ph_3P ligands on two opposite trigonal metal atoms: four long secondary interactions connect the two cycles. A much larger 28-membered cycle of alternating silver and sulfur atoms occurs in **10**, with the phosphine ligands on Ag^{trig} atoms 1, 6, 8, and 13. The cycle is folded such that its digonal and trigonal segments lie approximately in the faces of a box, with virtual symmetry C_{2h}. There are four types of segments in **10**: (i) eight opposed zigzag linear segments in opposite faces of the box; (ii) four linear crossover segments on another pair of faces; (iii) four trigonal bending segments, which connect to (iv) two linear end segments, one in each end of the box. Structural features that occur in these three compounds, as well as four other compounds with related but different structures, permit extraction of structural principles for copper(I) and silver(I) thiolate complexes with branched-chain alkyl substituents. Crystal data: **8**, $C_{52}H_{66}Cu_4S_4P_2$, space group $P2_1/c$, $a = 13.213$ (6) Å, $b = 27.242$ (8) Å, $c = 20.601$ (8) Å, $\beta = 130.57$ (1)°, $V = 5632$ (4) Å^3, $Z = 8$, 4068 observed ($I > 3\sigma(I)$) reflections (Mo Kα), $R = 0.045$; **9**, $C_{84}H_{134}Ag_8S_8P_2$, space group $P2_1/c$, $a = 14.736$ (8) Å, $b = 27.108$ (4) Å, $c = 24.94$ (2) Å, $\beta = 99.85$ (3)°, $V = 9815$ (8) Å^3, $Z = 4$, 5067 observed ($I > 3\sigma(I)$) reflections (Mo Kα), $R = 0.057$; **10**, $C_{128}H_{186}Ag_{14}S_{14}P_4(CHCl_3)_2$, space group $P\bar{1}$, $a = 13.523$ (8) Å, $b = 13.852$ (7) Å, $c = 21.808$ (12) Å, $\alpha = 79.86$ (4)°, $\beta = 86.08$ (4)°, $\gamma = 85.75$ (4)°, $V = 4004$ (4) Å^3, $Z = 1$, 2690 observed ($I > 3\sigma(I)$) reflections (Mo Kα), $R = 0.067$.

Introduction

Alkane- and arenethiolate compounds MSR of copper and silver are still incompletely characterized structurally, largely due to difficulties with insolubility and poor crystal habit, and there are only a few crystal structure determinations for this long-known class of compounds.[1] One approach to the problem has been to increase the steric bulk of the substituent R. Åkerström showed that multiple branching and bulk in the thiolate substituent enhanced the solubilities of $(MSR)_p$ in inert solvents and determined from ebullioscopic molecular weight measurements that silver

(1) Dance, I. G. *Polyhedron* **1986**, *5*, 1037.

0020-1669/89/1328-1853$01.50/0